Spontaneous Shift of Divertor Plasma Footprints during a Discharge in a Helical-Axis Heliotron Device

T. Mizuuchi 1), N. Nagata 1), H. Okada 1), G. Motojima 2), S. Kobayashi 1), K. Nagasaki 1), Z. Feng 3), N. Nishino 4), Y. Suzuki 5), M. Yokoyama 5), Y. Nakamura 2), S. Yamamoto 5), S. Watanabe 2), H. Arimoto 2), S. Matsuoka 2), M. Nosaku 2), T. Tomokiyo2), N. Watanabe 2), K. Hanatani 1), K. Kondo 2), F. Sano 1)

1) Institute of Advanced Energy, Kyoto University, Gokasho, Uji, Japan.
2) Graduate School of Energy Science, Kyoto University, Gokasho, Uji, Japan.
3) Southwestern Institute of Physics, Chengdu, China.
4) Graduate School of Engneering, Hiroshima University, Higashi-Hiroshima, Japan
5) National Institute for Fusion Science, Toki, Japan

e-mail contact of main author: mizuuchi@iae.kyoto-u.ac.jp

Abstract. A spontaneous shift of diverted plasma position during a discharge was investigated in Heliotron J. The shift of a few cm was observed for discharges with a non-inductive plasma current < 3 kA and the plasma stored energy < 3 kJ. The observed shift was related to the change in the plasma current more closely than the stored energy. The most plausible mechanism for the observed shift is the change of the edge field topology caused by the plasma current. The three-dimensional finite-β equilibrium calculations assuming profiles of plasma pressure and plasma current density indicate that the effect of the plasma current depends not only on the current flow direction but also on the current density profile. This experiment points out not only the importance of current control to fix the divertor plasma position in a low shear helical device but also the possibility of "divertor swing" for reduction of the divertor particle/heat load by controlling a small amount of plasma current within a tolerable influence on the plasma performance.

1. Introduction

Heliotron J [1, 2] is a low-magnetic-shear helical-axis heliotron device with an L = 1/M = 4 helical coil (R_0 = 1.2 m, $B_0 \leq$ 1.5 T), where L is the pole number of the helical coil and M is the pitch number of the field along the toroidal direction. The Heliotron J study aims at experimental exploration of the helical-axis heliotron concept [3] as an advanced helical device for fusion plasma confinement.

As experimentally demonstrated in W7-AS [4] and Heliotron J [5], the value of rotational transform $\iota/2\pi$ in a low shear device has great importance in the core plasma confinement including L-H transition. In addition, it is closely related with the edge field topology, which is to be used for a “built-in” divertor in helical systems. In the standard (STD) configuration of Heliotron J (the edge rotational transform $\iota(a)/2\pi \approx 0.56$), for example, the last closed flux surface (LCFS) is surrounded by “ergodic” field lines [6] and some parts of the “whisker” field lines outside the LCFS cross the vacuum chamber, forming “divertor traces” on the wall. When the edge rotational transform is set near a rational, 4/7 (≈ 0.57), complete (or non-complete) magnetic islands of n=4/m=7 surround LCFS and cause to modify the divertor field topology. Even in non-Ohmic heating plasmas, the plasma stored energy W_p and non-inductive plasma current I_p can affect $\iota(a)/2\pi$ and modify the divertor plasma distribution. Therefore, to use the intrinsic edge field topology for a divertor, it is important to experimentally study the dynamics of the divertor plasma distribution caused by the plasma discharge and its controllability.

This paper presents the experimental evidences of the modification of divertor plasma distribution during a discharge and discusses the mechanism of such modifications.

2. Experimental Setup

The details of the Heliotron J device is described in [1, 2]. For ECH discharges in this study, the plasma production and heating was performed by using the 70-GHz, 0.4-MW second harmonic X-mode ECH launching from a top port located in a straight section of Heliotron J [7], the toroidal angle of this section is defined as $\phi = 0.0°$ in this paper. The non-focused Gaussian beam diameter of the microwaves is ≈ 0.120 m at the magnetic axis in the launching section (about half of the plasma diameter on the equatorial plane). Due to the three-dimensional magnetic-axis configuration of Heliotron J, the parallel refractive index is $N_{//} \approx 0.44$ in the vacuum condition. For NBI experiments, the hydrogen beam ($E_{NBI} \sim 28$ kV, $P_{NBI} \sim 0.5$ MW) [8] was tangentially injected into a deuterium target plasma generated by the ECH. By selecting one of two beam-lines of NBI or changing the direction of the confinement field, co- or counter-injection experiments can be performed.

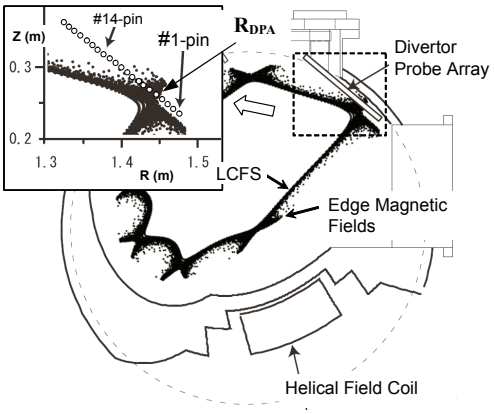

Fig. 1a Poincaré plot of the edge field lines at the divertor probe array section ($\phi = 67.5°$). The inset shows the probe-pin positions.

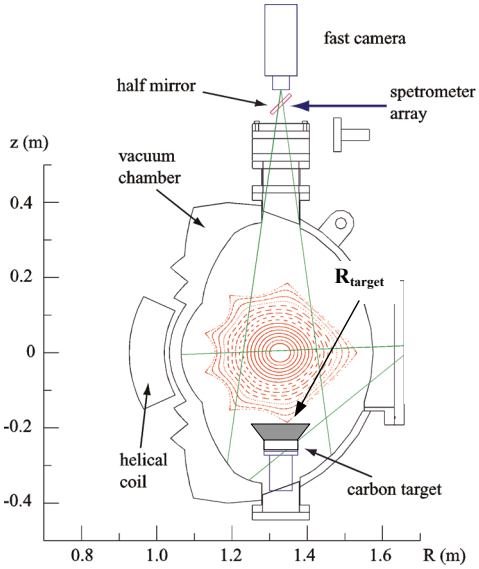

Fig.1b Schematic view of the rail-limiter type carbon target and the fast-camera image monitoring system.

In this study, the position (or spatial profile) of plasma flux outside LCFS was monitored by using two methods at different toroidal and poloidal positions. One is Langmuir probe measurements of the plasma flux coming to the wall along the intrinsic divertor field bundle by using poloidal probe-arrays installed near the wall (divertor probe array, DPA, Fig. 1a) at two toroidal sections ($\phi = 67.5°$ and $112.5°$ sections) [9], where the field topology is up-down symmetric each other. The distance of adjacent electrodes in each array is 10 mm on the array surface (about 7.7 mm in the major radius direction). Since the present array was designed for the field topology of the STD configuration of Heliotron J, the position of the array might not be the best one for some other configurations. Moreover, increasing of in-vessel equipments such as NBI beam-dumps, ICRF antenna, magnetic probes, armor tiles protecting some in-vessel diagnostics, might make their shadows on the probe arrays depending on the examined configuration. To compensate this disadvantage of the divertor probe measurement, the second method was additionally introduced in this study; two-dimensional measurement of the visible light image near a movable rail-limiter type carbon target (Fig. 1b), which was inserted from a bottom port of the device ($\phi = 157.5°$ section) and set at a proper position for each discharge condition to contact with the "whisker" of the edge field structure. An eight-bit digital video camera system, which was installed at the top port facing the target, was used for this measurement. Since the previous image measurements using a cannon-ball type target indicate that the brightness of the image near the target is well correlated to the plasma flux profile to the target [10], we consider the observed image with this rail-type target has profile information of the incoming plasma flux. The frame speed of this camera system is

250 or 500 fps and the numbers of pixel in a frame is 480 (for 250 fps) or 240(for 500 fps)×512 pixels. Depending on the brightness of the image, an exposure was set to 1/500 or 1/1000 of a second. At present camera setting, one pixel of the image data corresponds to about 1 mm. This paper focuses on the shift of the peak position of the brightness, R_{target}, rather than the detailed two-dimensional radiation profile near the leading-edge of the target.

3. Experiments

Figure 2 shows an example of time traces of the line-density of the core plasma ($n_e l$), intensity of Hα-emission (Hα), plasma stored energy (W_p), toroidal plasma current (I_p) and divertor plasma density measured by using one electrode of DPA(ϕ = 112.5°) at R ≈ 1.407 m for a discharge maintained by the combination of ECH (P_{ECH} ≈ 0.3 MW) and NBI (P_{NBI} ≈ 0.7 MW, co-injection) in the STD configuration. An increase in the growth rate of W_p and a sudden drop of Hα at ≈ 270 ms following slight decrease of Hα intensity from ≈ 255 ms indicate an appearance of L-H transition. (In this discharge, the target for the video camera measurement was not installed yet.) In this paper, we define the direction of the "positive" toroidal current as the direction where the plasma current increases the poloidal field by the coil system. The observed toroidal plasma current is gradually increases as increase of the stored energy. Since the plasma was produced during the quasi-steady state of the confinement field and one-turn voltage due to the drift of the external field strength was negligible, this current is non-inductive one. In the experimental condition at present, the non-inductive toroidal current can be driven by different three mechanisms [11]; bootstrap current, NB induced current (Ohkawa current) and EC driven current. In the density range shown in Fig. 2, the observed plasma current is considered to mainly consist of the bootstrap current and the NB induced current. The profiles of the diverted plasma density along the divertor probe array are shown in Fig. 3 as a function of the major radius at early (211 ms) and later (277 ms) timings of the discharge. The density distribution at 211 ms is consistent with that expected from the vacuum field topology if we take into account the ∇B-drift effects during the excursion of ions along the edge field lines to the probe, similar to that observed in low density ECH plasmas [9]. At 277 ms, the density peak position, R_{DPA}, along DPA clearly shifts inward about 4 cm compared to the position at 211 ms. The time trace of the shift of the density-peak position on DPA is shown in the bottom of Fig. 2. The overall trend of the density-peak-position shift seems to be well synchronized with the change of W_p or I_p. At the timing when the shift became its maximum, the value of the plasma current was about 2.7 kA.

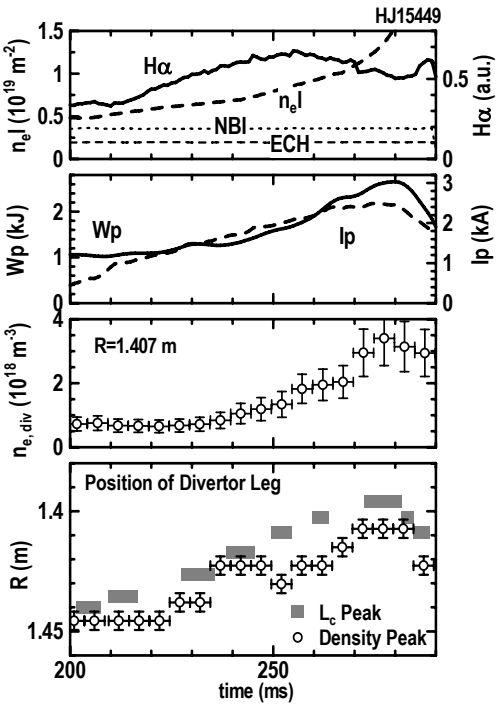

Fig. 2 Time traces of several signals for an ECH and NBI combination heating discharge in the STD configuration.

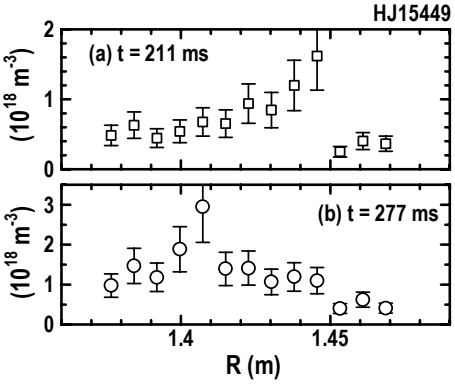

Fig. 3 Density profiles on the divertor probe array at two timing. (The same discharge as in Fig. 2.)

Figure 4 shows time traces of two shots from a discharge set of another ECH+NBI condition in the STD configuration. Similarly to the case shown in Fig. 2, the position of R_{DPA} gradually shifts inward as increase of W_p or I_p and goes back as decrease of W_p or I_p. Here, we use the peak position of the ion-saturation current profile as R_{DPA} on DPA(ϕ = 67.5°) instead of the density profile. The analysis of the visible light image near the target shows that the position of R_{target} also shifts inward/outward as increase/decrease of W_p or I_p. Here, the target was set at 0.215 m blow the equatorial plane (Z_t = -0.125 m). These observations at different toroidal and poloidal positions and different methods suggest the observed temporal shift of the peak edge-plasma position is not a local event but a global change of the edge plasma distribution during a discharge under the steady-state phase of the external field condition. It is interesting to note that W_p rapidly increases near 210 ms mainly due to the start of NBI but no clear jump in I_p. At this timing, there was no clear change in R_{target}, but as shown in the bottom of Fig. 4, there is a jump in R_{DPA} near the timing. This might suggest some local event near DPA. However, since the signal level of the probe was small in this phase and its profile was rather flat, we should be careful in the accuracy of the value of R_{DPA} around this timing and need more detailed investigations.

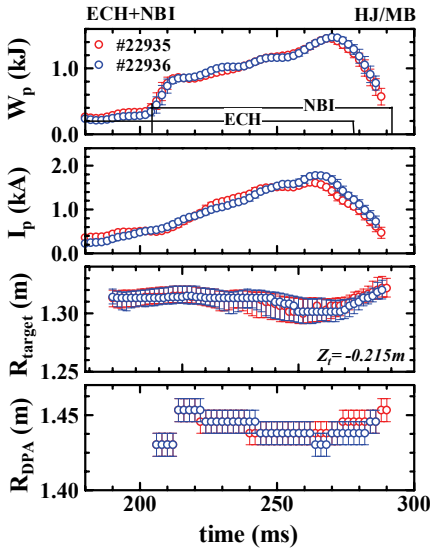

Fig. 4 Time traces of W_p, I_p, R_{target} and R_{DPA} for two ECH+NBI shots in the same discharge condition under the STD configuration.

Figure 5 shows another example of similar time traces as in Fig. 4 but for discharges sustained only by NBI (co-injection) in a High-Bumpiness (HB) configuration [12], where the magnetic axis is inwardly shifted about ~ 0.8 cm (on average along the torus) compared to that in the STD configuration. In this discharge condition, the direction of the confinement field was reversed (B < 0). Therefore, the "positive" direction of plasma current is opposite to that in the normal field (B > 0) discharge. The plasma current is driven by the plasma pressure and NBI also in this case. This example again shows temporal inward shifts of R_{target} and R_{DPA}. In the shot #23624, W_p and I_p were kept increasing up to almost the end of discharge, but in #23635, I_p started to decrease at t ~ 240 ms while W_p did not decrease and was kept almost the same value until the end of the NBI pulse. As shown in the figure, for #23635 discharge, the inward shifts of R_{target} and R_{DPA} were observed until t ~ 240 ms and they started to change the direction of shift for t > 240 ms, i.e. coming back to the values at the initial phase of the discharge. This and the no-response in R_{target} to the rapid change in W_p at t ~ 210 ms observed in Fig. 4 indicate that the shifts of R_{target} and R_{DPA} are more closely related to the change of plasma current.

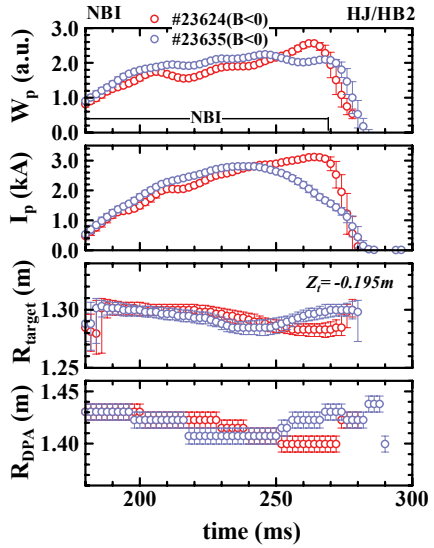

Fig. 5 Time traces of W_p, I_p, R_{target} and R_{DPA} for two NBI-only shots under the high-bumpiness configuration.

Figures 6(a) and (b) show the shifts of R_{DAP} and R_{target} observed in the cases of Figs. 4 and 5 as a

function of I_p, respectively. These figures indicate that the Ip-dependences of R_{target} and R_{DPA} are not described by linear functions. Comparing these two different discharge condition cases, it is found that the I_p-dependence seems sensitive in the case of Fig. 6(a), ECH+NBI discharge in the STD configuration. The shifts of R_{target}, and R_{DPA}, ΔR_{target} and ΔR_{DPA} are about 1.5 cm and 2.5 cm for $I_p \sim 1.7$ kA, respectively.

4. Discussions

The experiments show the temporal shift of R_{DPA} and R_{target}. Plausible candidates for the observed shifts are the change of the field topology caused by W_p and/or I_p. The plasma pressure can change the field topology through the shift of plasma column and the bootstrap current. However, only the simple outward shift of plasma column by W_p would cause the outward shift of the divertor trace on the outboard side of the torus. This is inconsistent with the observation shown in Figs. 2-5. Moreover, as shown in the previous section, the observed shift of edge plasma distribution is more closely related to the change in the plasma current than that in the stored energy. As for the effects of the plasma current, the observed non-inductive current is not so large and the change of $\iota(a)/2\pi$ would be small, for example, it would be about 0.007 for I_p of ~ 1 kA. Nevertheless, when the plasma current increases $\iota/2\pi$, the deformation of the field topology could become clearer since $\iota/2\pi$ comes near a rational 4/7.

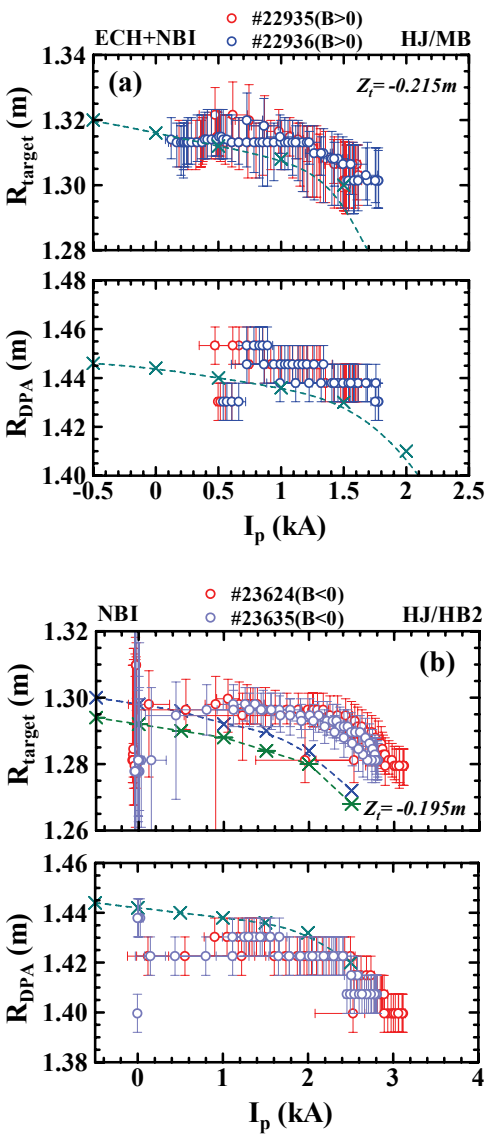

Fig. 6 (a) I_p-dependence of R_{target} and R_{DPA} for ECH+NBI plasmas in the STD configuration. The dataset is the same as that shown in Fig. 4. (b) I_p-dependence of R_{target} and R_{DPA} for NBI-only plasmas in the HB configuration. The dataset is the same as that shown in Fig. 5. The positions of L_c-peak from the calculation under the filament current assumption for DPA and the target are also plotted as a function of I_p. (see Sec. 4.)

As the first step of estimation of the plasma current effects on field topology, the modification of the vacuum field topology caused by the toroidal current was calculated assuming a filament current on the original vacuum magnetic axis. In this calculation, we evaluated the connection length L_c of the field line starting from the probe array or the leading edge of the target to the wall after traveling around the confinement region. It is a good measure of the plasma position on DPA [9] and the target unless the field line is not trapped in islands isolated from the confinement region. The position of L_c-peak is considered to correspond to the peak position of the diverted plasma profile when the ∇B-drift effect during the particle excursion is neglected.

Figure 7 shows the I_p-dependences of the radial position of L_c-peak on (a) the carbon target at Z_t = -0.215 m and (b) DPA for the STD configuration. It is found that the L_c-peak position for

both cases shifts inward for positive current ($I_p > 0$) and outward for negative current ($I_p < 0$). Their dependences are not a linear function and seems to increase for $|I_p| > 1.5$ kA.

The position of L_c-peak on DPA for the discharge shown in Fig. 2 is also plotted in the bottom of the figure as a function of time. Although there is a systematic discrepancy between the experimentally observed density-peak position and the L_c-peak position, it is observed the similar time dependence (therefore, the similar I_p-dependence) and almost the same span of shift for both of L_c-peak and R_{DPA}. In Fig. 6(a), the positions of L_c-peaks on the target and DPA are also plotted in the top and bottom figures, respectively. The data of Fig. 6(a) come from the discharges in the STD configuration and it is found again almost the same systematic discrepancy between $R_{DPA}(I_p)$ and L_c-peak(I_p) as that observed in the case of Fig. 2. Except for this discrepancy, the I_p-dependence of R_{DPA} qualitatively well agrees with that of L_c-peak position. As for the shift on the target, however, some difference between the measured R_{target} and L_c-peak position is observed. The shift of R_{target} seems to stay at a small value for the low current range ($I_p \leq 1.2$ kA), and then increases as increase of I_p with increasing rate close to that expected from the calculation.

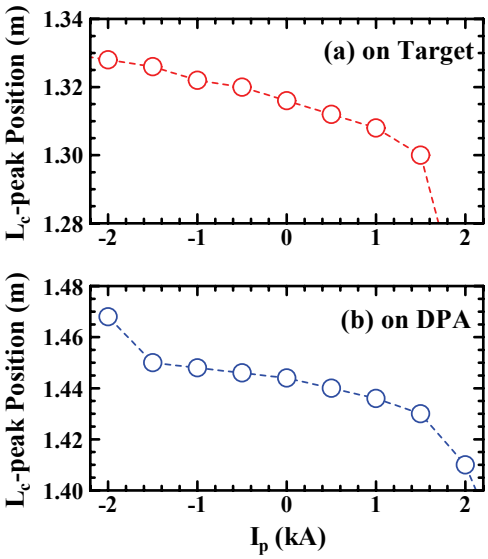

Fig. 7 I_p-dependences of the radial position of L_c-peak (a) on the carbon target (Z_t = -215 mm) and (b) on DPA for the STD configuration.

For the NBI-only discharges in the HB configuration shown in Fig. 5, the positions of L_c-peaks on the target and DPA are also plotted in the top and bottom figures of Fig. 6(b), respectively. The similar difference between R_{target} and L_c-peak position is observed also in these discharges.

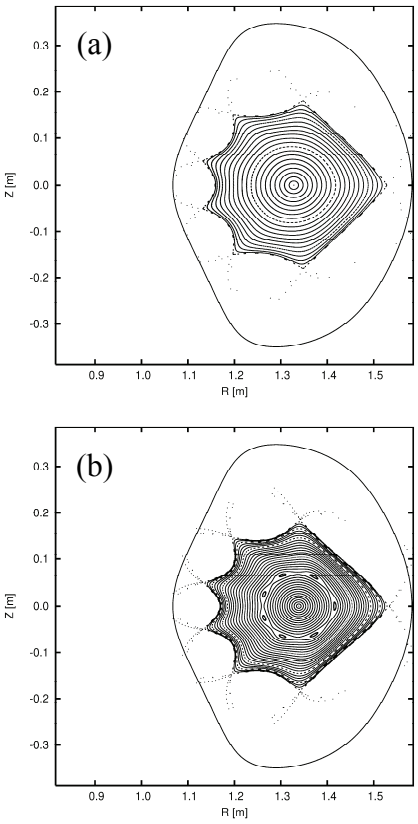

Fig. 8 Field topology at $\phi = 0°$ for the STD configuration in the cases of (a) $<\beta>=0$ % (vacuum) and (b) $<\beta> \sim 0.32$ %

More detailed three-dimensional equilibrium studies have been started through HINT2 [13] calculations. In the above discussions, we have ignored the deformation of the field topology caused by finite-β effect only. Figure 8 shows the field topology at $\phi = 0°$ including some whisker fields from HINT2 calculations for (a) $<\beta> = 0$ % (vacuum) and (b) ~ 0.32 % (roughly correspond to $W_p \sim 3$ kJ). Since we do not have enough profile data for the core plasma at present, we assume the plasma pressure profile of $p = p_0(1-s^2)^2$ in the calculation. As shown in the figure, at least in this low-β range, the size of LCFS becomes slightly smaller (see Fig. 9) but no remarkable deformation of field topology is observed except for the appearance of small is-

lands in the center region. The β-effect increases the rotational transform in the center region but changes little at the edge.

To understand the basic image of the effects caused by the toroidal current on the three-dimensional finite-β equilibrium, calculations were performed artificially adding toroidal current assuming three different current density profiles;

peaked $j = j_0(1-s)^8$,

flat $j = j_0(1-s^4)^2$

and

hollow $j = j_0(60(1-s^2)s^2-5(1-s^2))$

profiles. Here, the total net current was set at +2.0 or -2.0 kA. In the hollow profile case, the current in the core region of the confinement region flows to the direction reverse to that of the total net current. The calculated radial profile of the rotational transform is shown in Fig. 9 for each case. The figure indicates that the I_p-effect depends not only on its direction but also on the current density profile.

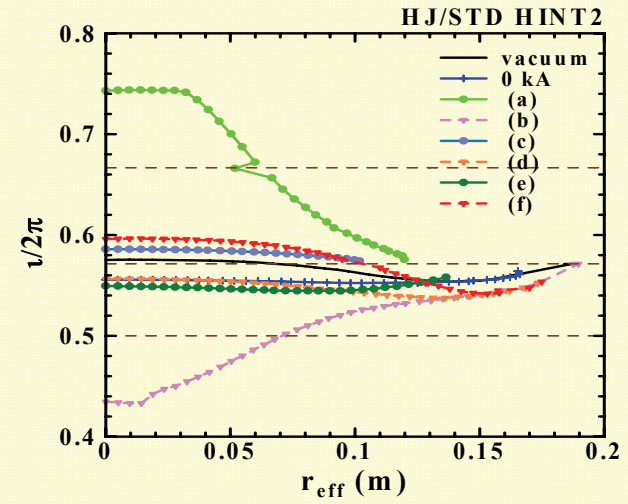

Fig. 9 Effects of plasma current on the rotational transform and the plasma radius for the STD configuration (from HINT2 calculation):
$<\beta> \sim 0.32$ %, $p=p_0(1-s^2)^2$
(a) $j = j_0(1-s)^8$, I_{net} = +2.0 kA
(b) $j = j_0(1-s)^8$, I_{net} = -2.0 kA
(c) $j = j_0(1-s^4)^2$, I_{net} = +2.0 kA
(d) $j = j_0(1-s^4)^2$, I_{net} = -2.0 kA
(e) $j = j_0(60(1-s^2)s^2-5(1-s^2))$, I_{net} = +2.0 kA
(f) $j = j_0(60(1-s^2)s^2-5(1-s^2))$, I_{net} = -2.0 kA

The current flowing in the positive direction changes the size of LCFS remarkably for all current profiles. Since the edge rotational transform in the STD configuration is ~0.56 in vacuum, it is interpreted that the approaching to a major resonance condition of $\iota/2\pi = 4/7$ caused by the positive current increases the "perturbed field area" and decreases the size of LCFS. On the other hand, the negative current, decreasing the rotational transform, could make enough room to expand the LCFS size without severe deformation of the edge topology. The change of the LCFS size can affect the whisker field position on a fixed observation plane and make the observed shift of plasma position on the plane since the distance of an "x-point" from the target changes. Similar effects were observed in $\iota/2\pi$-scan experiments performed in Heliotron E [14]. Since Heliotron E is a high shear heliotron device, the change of the rotational transform does not change the fish-tail shape of the divertor field structure and the footprints of the divertor fields on the wall expand or shrink in poloidally by increase or decrease of the distance between the x-point and the wall.

The HINT2 calculation predicts the change of the effective plasma size by the toroidal current in three-dimensional finite-β plasmas with toroidal current, besides the island formation inside LCFS. These effects would have a great impact on the evaluation of the global confinement property. Experimentally, we have no clear evidence at present, which directly indicates the modification of core plasma size itself. However, the observed shift of the edge plasma position presented in this paper might suggest the occurrence of plasma size deformation. It is an urgent task in Heliotron J experiment to obtain detailed profile data and directly check the plasma size.

It is important to note that the deformation of the edge field topology depends on the current density profile. The difference observed in the I_p-dependence of the R_{target} shift might be

originated from the temporal change of the current density profile. We have to be careful with the current density profile when we try to change the plasma current by any external method to control the I_p-effects on the field topology.

5. Summary

A spontaneous shift of diverted plasma position during a discharge is investigated in Heliotron J. For discharges with a non-inductive small plasma current ($I_p < 3$ kA) and the plasma stored energy ($W_p < 3$ kJ), the observed shift was an order of a few cm, which was measured by using the divertor probe array at the wall and the rail-limiter type carbon target touching with the whisker field lines of the plasma edge region. The observed shift is related to I_p more closely than W_p. The most plausible mechanism for the observed shift is the change of the edge field topology caused by I_p.

Model calculations for 3D finite-β equilibrium by HINT2 code were performed assuming profiles of plasma pressure and plasma current density profiles. The results indicate that the effect of the plasma current depends not only on its direction but also on the current profile.

This experiment points out not only the importance of current control to fix the divertor plasma position in a low shear helical device but also the possibility of "divertor swing" for reduction of the divertor particle/heat load by controlling a small amount of plasma current within a tolerable influence on plasma performance.

Acknowledgements

The authors are grateful to the Heliotron J supporting group for their excellent arrangement of the experiments. This work is performed with the support and under the auspices of the Collaboration Program of the Laboratory for Complex Energy Processes, IAE, Kyoto University and Kyoto University 21st century COE Program “Establishment of COE on Sustainable Energy System” as well as the NIFS Collaborative Research Program (NIFS04KUHL005 and NIFS04KUHL001-010).

References

[1] SANO, F., et al., J. Plasma and Fusion Res. SERIES **3** (2000) 26.
[2] OBIKI, T., et al., Nucl. Fusion **41** (2001) 833.
[3] WAKATANI, M., et al., Nucl. Fusion **40** (2000) 569.
[4] WAGNER, F., et al., 19th IAEA Fusion Energy Conference (Lyon, 2002), OV2-4.
[5] SANO, F., et al., Nucl. Fusion **45** (2005) 1557.
[6] MIZUUCHI, T., et al., J. Plasma and Fusion Res. SERIES **3** (2000) 192.
[7] SHIDARA, H., et al., Fusion Sci. Technol., Vol. **45**, Jan. 2004, p.41.
[8] KOBAYASHI, S., et al., 20th IAEA Fusion Energy Conference, (Vilamoura, Portugal, Nov. 2004), IAEA-CN-116/EX/P4-41.
[9] MIZUUCHI, T., et al., J. Nucl. Mater. **313-316** (2003) 947.
[10] NISHINO, N., et al., J. Nucl. Mater. **313-316** (2005) 1073.
[11] MOTOJIMA, G., et al., in print on Fusion Sci. Technol.
NAGASAKI, K., et al., in this conference EX/P6-14.
[12] MIZUUCHI, T., et al., Fusion Sci. Technol. **50** (2006) 352.
[13] SUZUKI. Y., et al., Nucl. Fusion **46** (2006) L19.
[14] MIZUUCHI, T., et al, J. Nucl. Mater. **176-177** (1990) 1070.